Heliyon 11 (2025) e41600

Contents lists available at ScienceDirect

Heliyon

journal homepage: www.cell.com/heliyon

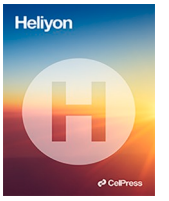

Research article

Construction of a novel cuproptosis-related gene signature and integrative analyses in cholangiocarcinoma

Liye Wang [a,1], Pan Li [b,1], Shuai Gong [a], Lina Pang [a], Mingyu Li [a], Chi Zhang [a], Shengli Zhang [a], Xiaoke Zhang [a], Guozhong Jiang [b], Wei He [a,*]

[a] Department of Oncology, The First Affiliated Hospital of Zhengzhou University, No.1 Eastern Jianshe Road, Zhengzhou, 450052, Henan, China
[b] Department of Pathology, The First Affiliated Hospital of Zhengzhou University, No.1 Eastern Jianshe Road, Zhengzhou, 450052, Henan, China

ARTICLE INFO

Keywords:
Cuproptosis
Cholangiocarcinoma
Molecular subtypes
Prognostic model
Tumor microenvironment
Drug sensitivity

ABSTRACT

Background: Cuproptosis is a unique form of cell death that is dependent on copper, which is fundamentally different from other recognized forms of cell death. However, the molecular and immune characteristics in cuproptosis-defined subgroups of cholangiocarcinoma (CCA) remain to be further illustrated.

Methods: We conducted a comprehensive investigation into the genetic and transcriptional variation, prognostic significance, and expression profiles of 16 cuproptosis-related genes (CRGs). To construct a prognostic signature based on differentially expressed genes between molecular subtypes, we employed LASSO and multivariate Cox regression analyses. We then assessed the values of this signature in prognostic prediction, immune infiltration, and therapeutic responses in CCA. The robustness of the signature was further validated in the GEO and IMvigor210 cohorts. Additionally, qRT-PCR and Western blotting (WB) were utilized to confirm the expression of the signature genes across different cell lines.

Results: A total of 16 CRGs were analyzed revealed differentially expressed, and two CRG-related clusters were identified, which displayed contrasting survival times.

Then, a robust cuproptosis-related risk model was established and was an independent prognostic factor for CCA, which was further validated across two external cohorts. Low-risk patients had a better overall survival than high-risk patients. The comprehensive results showed that a low-risk score was correlated with metabolism-related pathways, high infiltration of CD8 T cells, B cells, and M1 macrophages, active immunity and less aggressive phenotypes, high chemotherapeutic sensitivity, and more benefit from immunotherapy. In contrast, a high-risk score was associated with cancer and metastasis-related pathways, high infiltration of M2 macrophages, high expression of immune checkpoint genes, suppressive immunity and more aggressive phenotypes, and less benefit from chemotherapeutic and immunotherapy. In addition, the critical CRGs were further validated through qRT-PCR and WB.

Conclusions: We developed a novel risk model for CCA patients, which serves as a promising biomarker for distinguishing prognosis as well as molecular and immune characteristics.

* Corresponding author. The First Affiliated Hospital of Zhengzhou University No.1 Eastern Jianshe Road Zhengzhou, 450052, Henan, China.
E-mail address: hewei726@zzu.edu.cn (W. He).

[1] Liye Wang and Pan Li contributed equally to this work and share first authorship.

https://doi.org/10.1016/j.heliyon.2024.e41600
Received 4 August 2024; Received in revised form 18 November 2024; Accepted 30 December 2024
Available online 4 January 2025

1. Introduction

Cholangiocarcinoma (CCA) is a highly heterogeneous epithelial cell malignancy stemming from biliary epithelia and liver, with rising mortality worldwide over the past few decades [1]. According to the primary anatomic subtype, CCAs are classified into three categories: intrahepatic (iCCA), perihilar (pCCA), and distal (dCCA). CCA is asymptomatic in its early stage, leading to most CCA patients being diagnosed at advanced stages of the disease, where therapeutic options are severely limited [2]. Recent advances in treatments, such as surgical treatment, chemotherapy, and immunotherapy, have notably improved the prognosis of many patients with CCA [2,3]. However, most patients still tend to have unfavorable prognoses, with five-year overall survival (OS) rates lingering between 7 % and 20 %, which has garnered significant scientific and clinical interest [4]. What is more, sketchy molecular testing was conducted to guide CCA treatment [5]. The progress in identifying targeted genetic abnormalities in CCA highlights the emerging role of precision medicine in this disease. By employing transcriptomic analyses to identify gene signatures associated with CCA, which could provide a comprehensive evaluation of immune pathway-related signaling and tumor-related characteristics. Therefore, there is an urgent need to further explore distinct and practical molecular signatures that could enhance individualized treatment approaches and prognostic assessments for CCA.

Copper, an essential micronutrient, plays a pivotal role in numerous physiological processes within the human body, including cellular growth and proliferation [6]. However, the accumulation of excessive copper levels can lead to various cellular metabolic dysfunctions, ultimately resulting in cell death [7]. It is well known that copper is also required for cancer cell proliferation, tumor angiogenesis, as well as metastasis [8]. Elevated copper levels have been observed in a variety of malignancies compared to normal patients, including lung cancer [9], breast cancer [10], carcinoma of gallbladder [11] and so on. Further, copper has the potential to diminish the abundance of 60S ribosomal subunits while impairing rRNA processing, thereby enhancing the sensitivity of CCA cells to tripterine [12]. In recent years, a novel form of cell death termed cuprotosis has been identified, which is characterized by the direct binding to fatty acylation components in the tricarboxylic acid cycle (TCA cycle) [13]. When respiring, the accumulation of lipoylated TCA enzymes occurs, leading to the abnormal aggregation and imbalance of these proteins, which effectively obstructs the TCA cycle, inducing inevitably acute proteotoxic stress, culminating in cell death [13]. Cuprotosis is recognized as a copper-dependent form of cell death [14], which is distinct from other known death mechanisms such as ferroptosis, pyroptosis, and necroptosis. Multiple studies [15,16] highlighted the prognostic significance and molecular subtypes associated with cuproptosis-related genes, which may pave the way for developing innovative therapeutic strategies. However, the precise role of cuprotosis in CCA remains to be clarified.

In this study, we aim to comprehensively explore the various aspects of cuproptosis-related genes (CRGs) and to establish a cuproptosis-related prognostic signature in CCA. We further analyzed this cuproptosis-related signature in association with prognosis, tumor microenvironment (TME) infiltration, and treatment responses in CCA samples by utilizing high-dimensional datasets from E-MTAB. The results were further verified and supplemented using the GEO and IMvigor210 datasets. The results were also verified in cell lines through quantitative real-time PCR (qRT-PCR) and Western blotting (WB).

2. Materials and methods

2.1. Patients and datasets

RNA-seq data (FPKM value) of 53 CCA samples, including 44 cancer samples and 9 para-cancer samples were downloaded from the Cancer Genome Atlas (TCGA) database (https://portal.gdc.cancer.gov/, accessed in November 25, 2023). Single-nucleotide variant (SNV) data and copy number variation (CNV) data were also obtained from TCGA database. A total of 75 tumor samples and 29 normal samples, and their clinicopathological information in the E-MTAB-6389 cohort was available on the ArrayExpress website (https://www.ebi.ac.uk/arrayexpress/). GSE244807 dataset (https://www.ncbi.nlm.nih.gov/geo/query/acc.cgi?acc=GSE244807) was used as the validation cohort. The gene expression profiles and survival data of CCA patients in this dataset were obtained from Gene Expression Omnibus database (GEO, http://www.ncbi.nlm.nih.gov/geo). For all included RNA-seq data, normalization and log2 (x +1) transformation were performed. The mRNA transcriptome profiling and corresponding clinical data of the IMvigor210 cohort were extracted from http://research-pub.gene.com/IMvigor210CoreBiologies. The clinical samples lacking survival status or OS were excluded for further analysis.

A total of 16 CRGs were identified based on the previous study [13], which included 10 genes discovered through whole-genome CRISPR/Cas9 screen analysis, 3 Cu transporter-related genes, and 3 TCA cycle-related genes. Raw sequencing data were downloaded from the E-MTAB-6389 dataset. Reads were first trimmed using Trimmomatic (version 0.39) to remove low quality bases and adaptor sequences [17]. Samtools (version 1.9) was used to sort the reads coordinates [18]. Normalize the alignment data using the BamCoverage function of deepTools (version 3.5.0) [19]. Finally, gene lists were exported and intersected for further analysis.

2.2. Molecular characterization of CRGs in CCA

The mutation frequency and corresponding waterfall plot for 16 CRGs in CCA samples were illustrated utilizing the R maftools package. The frequency of CNV was presented through a cleveland dot plot by the ggpubr package. The distribution of the 16 CRGs across 23 chromosomes was visualized using the circlize package. To compare the differential expression of 16 CRGs between the tumor and normal samples, the limma and ggpubr packages were employed. Additionally, X-tile software (version 3.6.1; Yale University, New Haven, CT, USA) [20] was utilized to determine the optimal cut-off values for CRGs based on the associations with patient OS. We performed statistical test and plotted the Kaplan-Meier (K-M) curve to determine the prognostic value of single CRG in CCA

using limma, survival, and survminer packages. The igraph package was used to calculate and visualize the correlations between expression levels of CRGs. Univariate and multivariate Cox regression analysis for OS was performed in CCA. The forest plot of each variable was visualized by the forestplot package. Gene Ontology (GO) and Kyoto Encyclopedia of Genes and Genomes (KEGG) analysis of CRGs were analyzed by the clusterProfiler package.

2.3. Construction of cuproptosis-related clusters

The advantage of non-negative matrix factorization (NMF) in gene expression data analysis lies in its ability to identify localized gene expression features that are dominated by a small number of functional categories, suggesting that they are groupings of genetic components based on cell function. The novelty of this approach relative to other clustering methods is that NMF generates clusters based on local patterns, grouping together sets of genes with strongly correlated behaviors only in subsets of the data [21]. Based on the expression levels of CRGs, we employed a NMF approach to categorize patients into distinct clusters associated with cuproptosis utilizing the ConsensusClusterPlus package. The optimal number of clusters was established through analysis of the consensus matrix heatmap and cophenetic correlation coefficient. Principal component analysis (PCA) was performed to validate the robustness and reliability of the established CRG clusters.

2.4. Estimation of gene set enrichment analysis and tumor microenvironment cell infiltration between CRG clusters

Gene set variation analysis (GSVA) was conducted to investigate the difference of the biological function between CRG clusters using GSVA package of R and "c2.cp.kegg.v7.5.symbols". Single sample gene set enrichment analysis (ssGSEA) analysis was then conducted to assess the presence of immune cells and the associated immune functions within the tumor immune microenvironment. To analyze the ratio of immune-stromal components in this environment, we employed the estimate package in R. Furthermore, we compared the immune scores across the different CRG clusters. Moreover, tumor immune dysfunction and exclusion (TIDE) score was calculated online (http://tide.dfci.harvard.edu/) [22], including integrated TIDE score, microsatellite instability (MSI) score, dysfunction, and exclusion of each CCA sample.

2.5. Identification of differentially expressed genes between CRG clusters and construction of cuproptosis gene clusters

Based on between different CRG clusters, lists of differentially expressed genes (p-value <0.05, $|\log2(\text{FoldChange})| > 0.585$) were identified by using the limma package. In the signaling pathway analysis, CRG cluster-related DEGs were carried out by using the GSEA method based on the KEGG with the clusterProfiler package and “c2.cp.kegg.Hs.symbols”. Univariate Cox analysis was conducted on DEGs to identify DEGs that were associated with OS (p value < 0.05), which were subsequently selected for further investigation. The NMF analysis was then performed on the expression levels of OS-related DEGs to divided patients into distinct clusters based on cuproptosis gene expression, employing the R package ConsensusClusterPlus. Additionally, Kaplan-Meier analysis was utilized to examine survival differences among the identified clusters.

2.6. Construction of the cuproptosis-related scoring prognostic model

The least absolute shrinkage and selection operator (LASSO) Cox regression were performed on OS-related DEGs to reduce the dimension of high-latitude data using glmnet package. Subsequently, we performed a multivariate Cox regression analysis on the DEGs identified through the LASSO regression analysis. Finally, we determined the risk score for each patient by employing the following formula:

Risk score=(coefficient A) * exp A+ (coefficient B) * exp B+ … … + (coefficient N) * exp N. The coefficient N and exp N in the formula represent the coefficient index and expression level of genes, respectively.

X-tile software was employed to identify the optimal cut-off values that differentiate between high- and low-risk groups, utilizing the relationships with patient OS. Patients categorized with a high-risk score (E-MTAB-6389 > 1.52, GSE244807 > 5.69) were assigned as the high-risk group, while those with a low-risk score (E-MTAB-6389 ≤ 1.52, GSE244807 ≤ 5.69) were classified into the low-risk group.

Subsequently, a Kaplan-Meier analysis was performed to evaluate the survival probability between the two risk groups utilizing the survival and survminer packages.

Receiver operating characteristic (ROC) curves were generated to predictive the accuracy of this model, and the area under the curve (AUC) values for 1-, 3-, and 5-year survival were calculated using the timeROC package. The external cohort GSE244807 was employed to validate the risk score prognostic model. Furthermore, univariate and multivariate Cox regression analyses were conducted to ascertain whether the risk score could be regarded as an independent prognostic factor. Additionally, a sankey diagram was utilized to illustrate the distribution of patients across CRG clusters, risk scores, and their corresponding survival status.

2.7. Correlations of cuproptosis-related risk score with immune infiltrates and immune checkpoint genes (ICGs) in CCA

Enrichment analysis to determine the signaling pathways differences between high- and low-risk groups, GSEA was performed. We then employed R package ESTIMATE to evaluate the relative proportion of 22 types of immune cells. Then, we analyzed the spearman correlation between the relative proportions of immune cells and the risk score, and compared the differences of ICGs between the risk

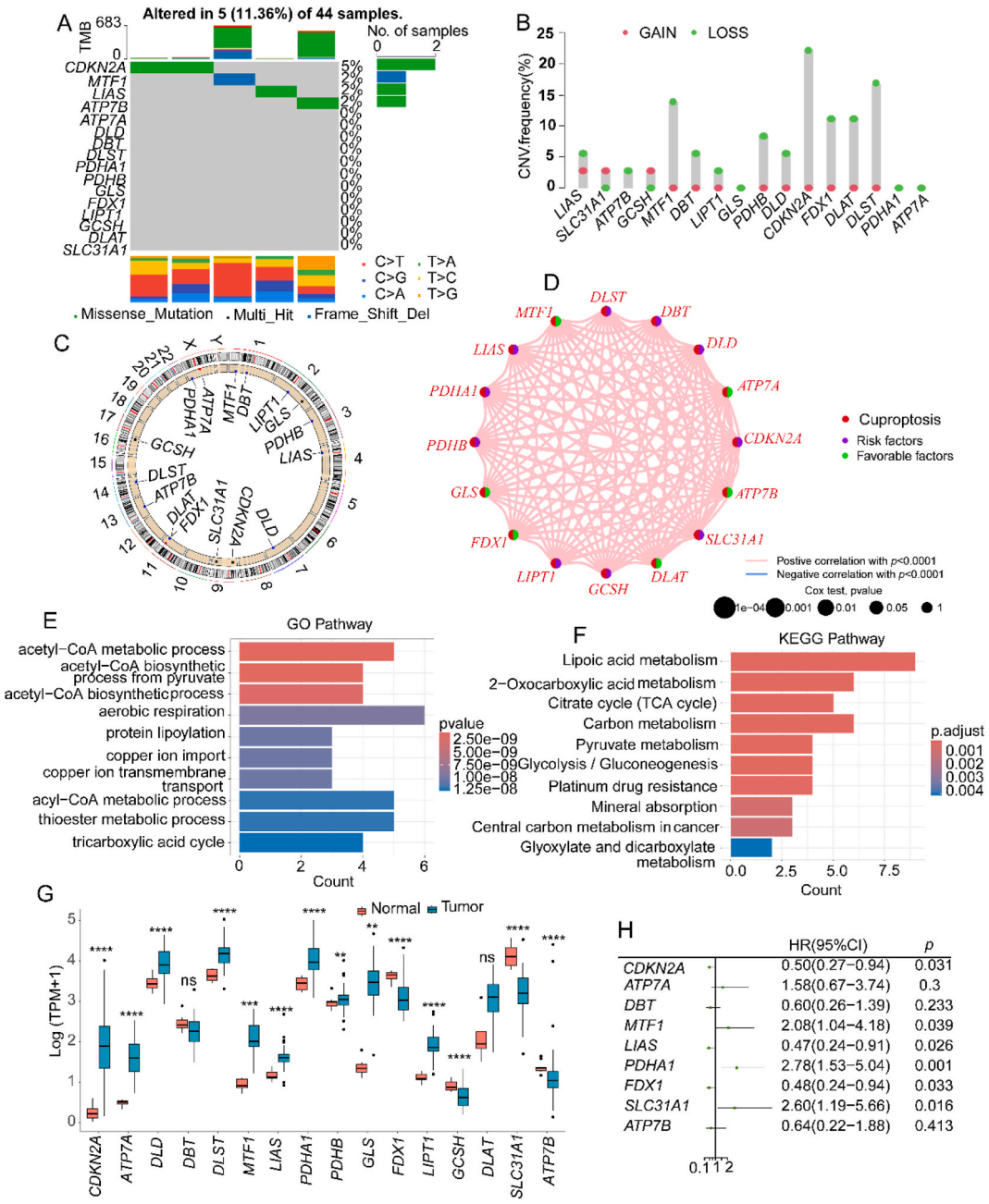

Fig. 1. Landscape of genetic and transcriptional alterations of cuproptosis-related genes (CRGs) in CCA. (A) The landscape of mutation profiles of 44 CCA patients from TCGA-CHOL cohort. Mutated genes (rows, 16 CRGs) are ordered by mutation rate. The right shows mutation percentage, and the top shows the overall number of mutations. The color-coding indicates the mutation type. (B) The CNV frequency of CRGs in TCGA-CHOL cohort. (C) The circus plot showed the location of CNV alteration of CRGs on 23 chromosomes. (D) The network showed interactions among CRGs in TCGA-CHOL cohort. (E) The top 10 enriched items of CRGs in GO analysis in biological process. (F) The top 10 enriched pathways of CRGs in KEGG database. (G) Differences in the expression levels of 16 CRGs between tumor and normal samples in TCGA-CHOL cohort. (H) Multivariate cox regression analysis of 9 CRGs associated with overall survival in E-MTAB-6389 cohort. CCA, CHOL: cholangiocarcinoma; CNV: copy number variation; GO: gene ontology; KEGG: Kyoto Encyclopedia of Genes and Genomes; TCGA: the Cancer Genome Atlas. ns: not significant, *$p < 0.05$, **$p < 0.01$, ***$p < 0.001$, ****$p < 0.0001$.

score groups. Then, we compared the ratio of immune-stromal components between different risk groups.

2.8. Estimation of cuproptosis-related risk prognostic model in immunotherapy response and chemotherapeutic sensitivity

The TIDE score, calculated through an online platform, serves as a valuable tool in identifying patients who are more likely to benefit from immunotherapy. In addition, the IMvigor210 cohort [23] was utilized to validate the predictive capability of the cuproptosis-related risk prognostic model in assessing responses to immunotherapy. The difference in risk scores between complete

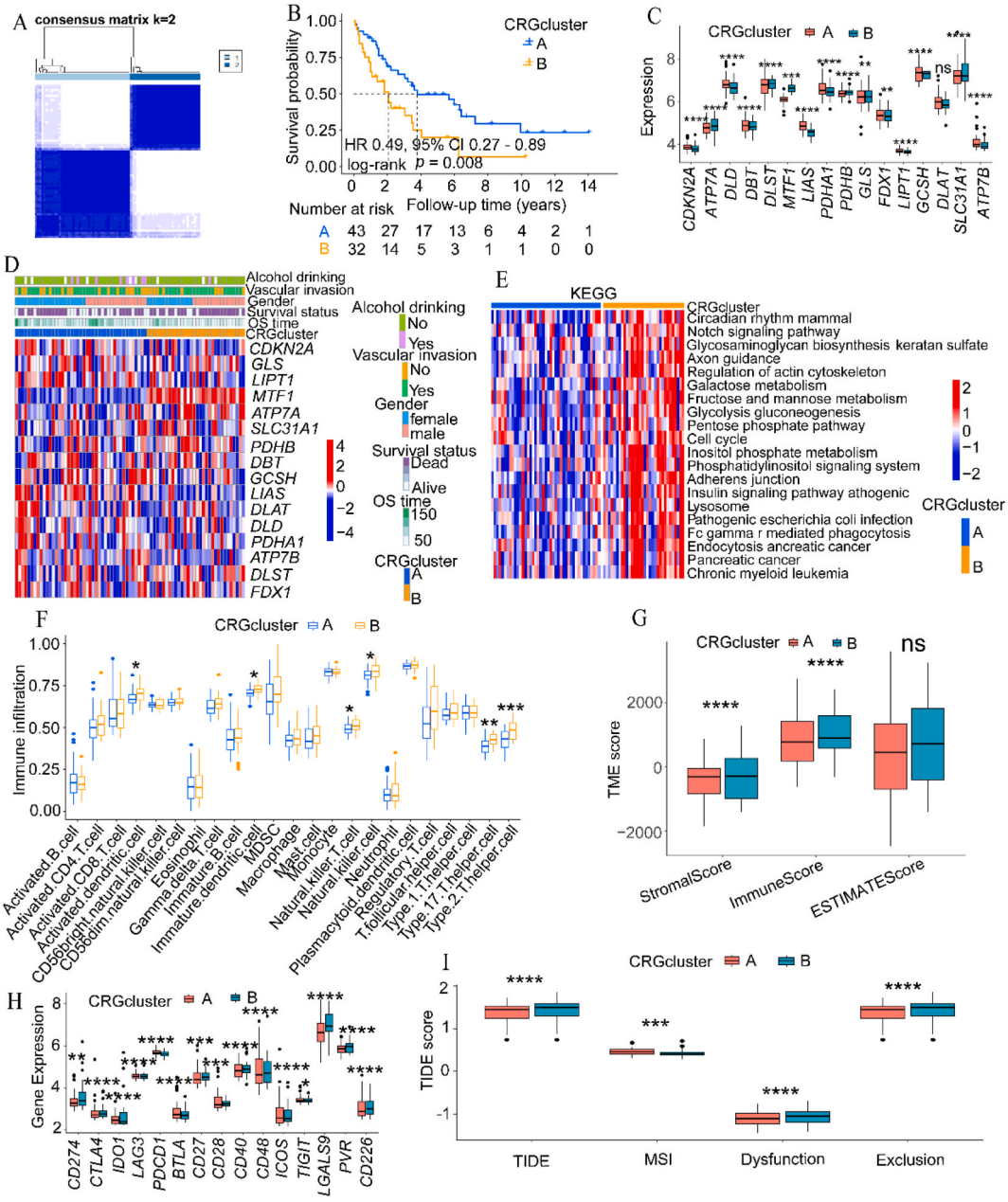

Fig. 2. Correlations of CRG clusters with clinical features, tumor microenvironment (TME), immune checkpoint genes (ICGs), and tumor immune dysfunction and exclusion (TIDE) score. (A) Consensus matrix of nonnegative matrix factorization (NMF) analysis. (B) The K-M plot of the two CRG clusters. (C) Differential expression of CRGs between CRG clusters. (D) The heatmap showed the different expressions of CRGs and clinicopathological characteristics between CRG clusters. (E) Gene set variation analysis (GSVA) heatmap of the two CRG clusters. (F) The single sample gene set enrichment analysis (ssGSEA) analysis of the two CRG clusters. (G) Correlations between the two CRG clusters and TME scores. (H) The different expressions of ICGs between CRG clusters. (I) TIDE score of the two CRG clusters. CRG: cuproptosis-related genes; OS: overall survival; KEGG: Kyoto Encyclopedia of Genes and Genomes; ns: not significant, $*p < 0.05$, $**p < 0.01$, $***p < 0.001$, $****p < 0.0001$.

response (CR)/partial response (PR) and stable disease (SD)/progressive disease (PD) was compared. The gene expression and drug sensitivity data for predicting drug responses were downloaded from the Genomics of Drug Sensitivity in Cancer website (GDSC, https://www.cancerrxgene.org). To calculate the half-maximal inhibitory concentration (IC50) values for anti-CCA agents, we employed the calcPhenotype function of the oncoPblueict R package. The lower-IC50 indicates more sensitivity to the drug.

2.9. RNA extraction and quantitative real-time PCR

Total RNA was extracted by Trizol reagent (ThermoFisher: #15596018) according to the manufacturer's protocol. The PrimeScript RT reagent kit (EZBioscience: #A0010CGQ) and SYBR-Green PCR reagent (ThermoFisher: # 4309155) were used to perform cDNA synthetization and analysis. The housekeeping gene GAPDH was utilized as an internal control. The primers used for RT-qPCR are shown in Table S1. The $2^{-\Delta\Delta Ct}$ method was applied to calculate the relative expression levels of genes.

2.10. Western blotting (WB)

The expression levels of critical CRMs were verified through Western blotting (WB). Cells were lysed using radioimmunoprecipitation assay (RIPA) buffer, and the total protein samples were subsequently subjected to separation via 10 % Tris-Tricine SDS-PAGE, followed by transfer onto a polyvinylidene fluoride (PVDF) membrane. After blocking with skim milk in TBST for 2 h, the PVDF membrane was incubated overnight at 4 °C with the primary antibody (*RAB3B*: Cohesion, #CQA9216; *KIAA0754*: Proteintech, #13058-1-AP; *FBXO32*: Cohesion, #CQA1166). After washing the membrane 3 times, it was incubated with horseradish peroxidase (HRP)-conjugated secondary antibody for 1 h at 37 °C. Subsequently, the membrane was developed using ECL solution, and the resulting bands were visualized with a ChemiDoc™ Imaging System.

2.11. Statistical analysis

qRT-PCR and WB were repeated at least 3 times. Statistical analyses were performed with software programs (SPSS version 26.0 (IBM); R version 4.3.1; GraphPad Prism 8). To compare variables between groups were assessed using the Mann-Whitney *U* test, *t*-test or one-way Anova for continuous variables. The Kaplan-Meier method was employed to conduct survival analysis, with differences assessed using the log-rank test. For the correlation analysis of continuous data, the Spearman test was utilized. All statistical tests were two-sided, and $p < 0.05$ was considered to have the statistically significant difference.

3. Results

3.1. Overview of molecular characterization of CRGs in CCA

In our study, we identified a total of 16 CRGs as reported by Tsvetkov et al. [13]. Of the 44 CCA patients in the TCGA cohort were used to analysis the somatic mutations and CNVs of CRGs in CCA. The genetic mutation landscape of CRGs was observed in 5 of 44 (11.36 %) CCA samples (Fig. 1A). Missense mutations were the most common mutation type, followed by frameshift deletion. We found *CDKN2A* had the highest mutation frequency (5 %), followed by *MTF1*, *LIAS*, *ATP7B*. Next, we analyzed the frequencies of the CNVs of 16 CRGs in CCA (Fig. 1B). The amplification frequency of *LIAS*, *SLC31A1* and *GCSH* were the highest, while *CDKN2A* had the highest loss frequency of CNV. The location of the CNV alterations of 16 CRGs on 23 chromosomes were shown in Fig. 1C. In addition, we explored the molecular interactions between CRGs. We found high expression levels of *PDHB*, *PDHA1*, *LIAS*, *DLST*, *DBT*, *DLD*, *CDKN2A*, *SLC31A1*, *GCSH* and *LIPT1* were the risk factors for CCA patients (Fig. 1D).

To further elucidate the role of CRGs, we conducted an in-depth investigation through GO and KEGG enrichment analyses. We found that the GO analysis demonstrated significant enrichment related to the acetyl-CoA metabolic process, aerobic respiration, copper ion import (Fig. 1E). KEGG pathway analysis were significantly enriched in the lipoic acid metabolism, 2-Oxocarboxylic acid metabolism, TCA cycle and platinum drug resistance (Fig. 1F). Subsequently, we investigated the expression of 16 CRGs both in the TCGA-CHOL samples and normal samples. Compared to normal tissues, significantly higher expression for *CDKN2A*, *ATP7A*, *DLD*, *DLST*, *MTF1*, *LIAS*, *PDHA1*, *PDHB*, *GLS*, *LIPT1* in tumor tissues (Fig. 1G). Seven prognostic CRGs were identified by Kaplan-Meier analysis (Fig. S1) and univariate Cox regression analysis (Fig. S2). As a result, multivariate Cox regression analysis further revealed that *CDKN2A*, *MTF1*, *LIAS*, *PDHA1*, *FDX1* and *SLC31A1* were independent prognostic factors (Fig. 1H).

3.2. Construction of CRG clusters in CCA

To further analyze the expression features and potential biological characteristics, we used the consensus clustering algorithm to categorize patients with CCA within the E-MTAB-6389 cohort. Utilizing the expression profiles of 16 CRGs, we successfully classified the patients into two distinct groups: CRG cluster A (n = 43) and CRG cluster B (n = 32) (Fig. 2A, Figs. S3A–H). The PCA analysis demonstrated that CCA samples were obvious categorized into two clusters (Fig. S3I). The Kaplan-Meier survival analysis showed that the patients with cluster A had better OS than patients with cluster B (Fig. 2B). In addition, CRGs including *CDKN2A*, *DLD*, *DBT*, *LIAS*, *PDHA1*, *FDX1*, *LIPT1*, *GCSH*, *ATP7B* were significantly higher expressed in cluster A, while *ATP7A*, *DLST*, *MTF1*, *PDHB*, *GLS*, *SLC31A1* were significantly higher expressed in cluster B (Fig. 2C). Fig. 2D illustrated the varying expressions of CRGs along with the associated clinicopathological characteristics between CRG cluster A and B.

3.3. Correlations of CRG clusters with tumor microenvironment and immune checkpoint genes (ICGs)

The GSVA analysis showed the different activation of KEGG pathways between two CRG clusters (Fig. 2E). We observed that notch signaling pathway, glycolysis gluconeogenesis, cell cycle, and pancreatic cancer were significantly enriched in cluster B. To examine the immune infiltration composition in different CRG cluster subgroups, we utilized ssGSEA and immune-stromal ratio algorithms to compare the relative abundance of immune cells and assess the tumor microenvironment (TME) score. We found that activated dendritic cell, immature dendritic cell, natural killer T cell, natural killer cell, type 17 T helper cell and type 2 T helper cell were differentially infiltrated between two CRG clusters (Fig. 2F). Meanwhile, the StromalScore and the ImmuneScore of cluster B were higher than cluster A (Fig. 2G). Next, we further observed that ICGs including *CD274*, *CTLA4*, *CD27*, *CD28*, *CD40*, *CD48*, *LGALS9*, *PVR* and *CD226* were significantly expressed lower in cluster A than cluster B (Fig. 2H). Moreover, integrated TIDE score, the dysfunction score and the exclusion score were significantly higher in cluster B, while the microsatellite instability (MSI) score was higher in cluster A (Fig. 2I). These findings suggested that the TME influenced by the two CRG clusters exhibits notable differences.

3.4. Identification of cuproptosis gene clusters in CCA

In differential expression analysis in the E-MTAB-6389 cohort, a total of 16 CRG cluster-related DEGs were obtained. GSEA were performed on these DEGs showed that CRG cluster A was mainly abundant in metabolism-related pathways (Fig. 3A), and CRG cluster B was abundant in arrhythmogenic right ventricular cardiomyopathy arvc, cancer-related pathways (pathways in cancer, P53 signaling pathway), and cell cycle (Fig. 3B). Subsequently, we performed univariate Cox regression analysis on the DEGs associated

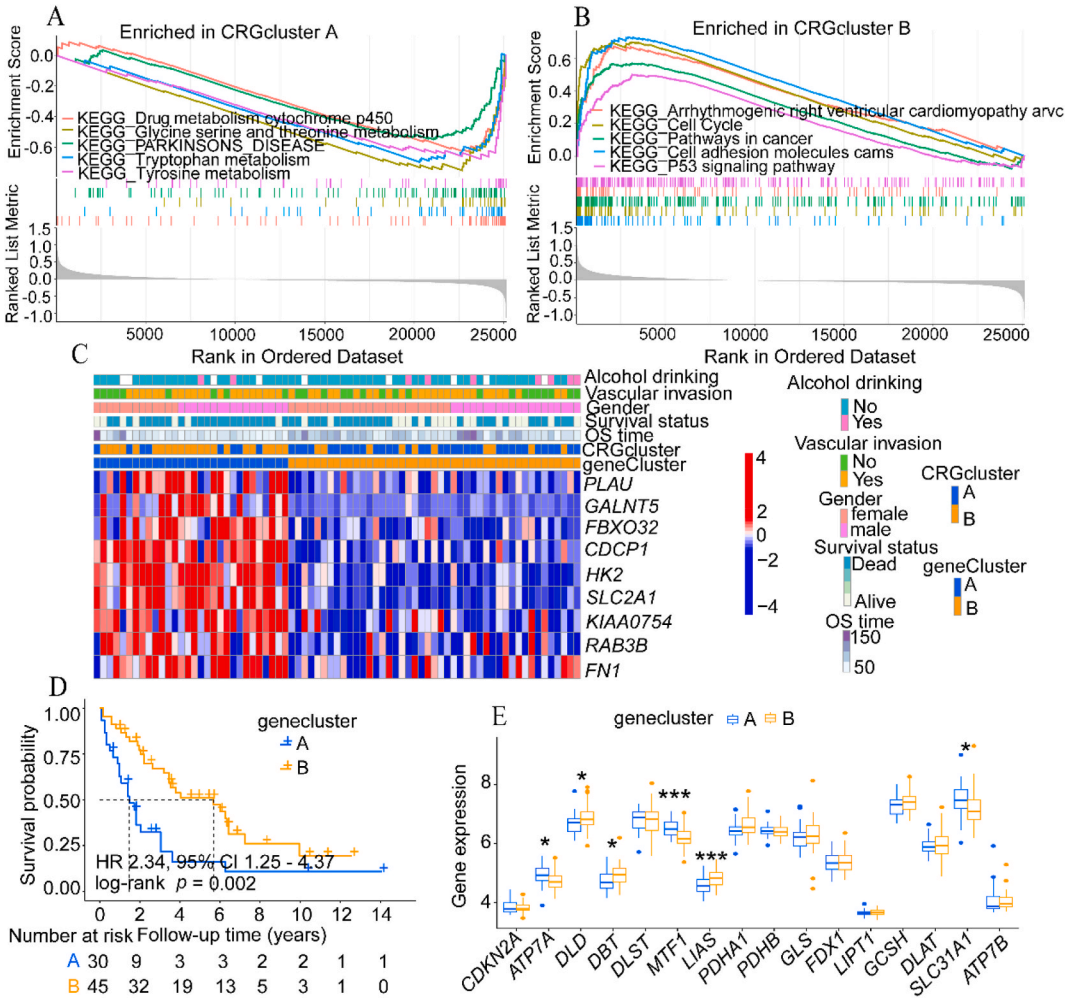

Fig. 3. Function enrichment in cuproptosis-related gene (CRG) clusters and construction of cuproptosis gene clusters. Gene set enrichment analysis (GSEA) enriched in CRG cluster A (A) and cluster B (B). (C) The heatmap showed the different expressions of overall survival (OS)-DEGs and clinicopathological characteristics between gene clusters. (D) The K-M plot of the two gene clusters. (E) Differential expression of CRGs between gene clusters. KEGG: Kyoto Encyclopedia of Genes and Genomes; $^{*}p < 0.05$, $^{***}p < 0.001$.

with the CRG clusters, identifying a total of 9-genes associated with OS (OS-related DEGs, $p < 0.05$). Utilizing the expression profiles of these OS-related DEGs, we distinguished two distinct clusters through NMF-clustering analysis (Figs. S4A–I). Fig. 3C illustrated the variations in the expression of OS-DEGs alongside the clinicopathological characteristics delineated between the cuproptosis gene clusters. Notably, gene cluster A exhibited a significant correlation with elevated expression levels and a greater number of mortality events. As shown in Fig. 3D, the patients with gene cluster B had better OS than patients with gene cluster A. Furthermore, CRGs including *DLD*, *DBT* and *LIAS* were significantly higher expressed in gene cluster B, while *ATP7A*, *MTF1* and *SLC31A1* were the opposite (Fig. 3E).

3.5. Construction and validation of the cuproptosis-related risk prognostic model

LASSO (Figs. S5A and B) and multivariate Cox regression analysis of the 9 OS-related DEGs showed that *RAB3B*, *KIAA0754*, and *FBXO32* were independent prognostic factors. Next, we constructed a 3-gene risk prognostic model as follows: Risk score = 0.321256***RAB3B*+0.410032***KIAA0754* + 0.343371***FBXO32*. X-tile software was utilized to identify the optimal cut-off values within the E-MTAB-6389 cohort (cutoff = 1.52) and the GSE244807 cohort (cutoff = 5.69). Subsequently, the CCA samples were categorized into high- and low-risk groups based on the cut-off values.

As illustrated in Fig. 4A and B, an increase in risk score was associated with a higher incidence of mortality and a reduction in survival time among patients.

The heatmap showed the different expressions of *RAB3B*, *KIAA0754*, and *FBXO32* between the high- and low-risk groups in E-MTAB-6389 cohort and GSE244807 cohort. In addition, Kaplan-Meier analysis showed that patients in low-risk group was superior to these in high-risk group in both E-MTAB-6389 cohort (Fig. 4C) and GSE244807 cohort (Fig. 4D). Furthermore, the risk score model prediction accuracy evaluated by the AUC of 1-, 3-, and 5-year was 0.741, 0.802, and 0.79, respectively, in the E-MTAB-6389 cohort (Fig. 4E). In the GSE244807 cohort, AUC values for predicting 1-, 3-, and 5-year OS were 0.548, 0.553, and 0.502 (Fig. 4F). The Sankey diagram showed the distribution of patients by CRG clusters, risk score, and survival outcomes are represented in Fig. 4G.

Meanwhile, we found that risk scores in CRG cluster B were significantly higher than that in CRG cluster A (Fig. 4H), while in gene cluster A were significantly higher than that in gene cluster B (Fig. 4I). Moreover, the expression of CRGs including *ATP7A*, *DLST*, *MTF1*, *PDHB*, *SLC31A1* were significantly higher in the high-risk group, while others were the opposite (Fig. 4J). Univariate (Fig. 5A) and multivariate (Fig. 5B) Cox regression analysis further revealed that the risk score was an independent prognostic factor.

3.6. Immune characteristics of different risk score subgroups

In order to further explore the biological characteristics between risk score subgroups, GSEA and CIBERSORT were performed. The results of the GSEA of KEGG terms showed that low-risk subgroup was mainly significantly enriched in metabolism-related pathways (Fig. 5C), and high-risk subgroup was significantly abundant in Fc gamma r mediated phagocytosis, cancer-related pathways (pathways in cancer, MAPK signaling pathway), cell adhesion and migration pathways (Fig. 5D). We further investigated the correlation of immune cells infiltration with risk score (Fig. 5E). Macrophages M2, neutrophils, and NK cells activated were positively correlated with risk score, while T cells gamma delta and T cells CD4 memory resting were negatively correlated with risk score. Meanwhile, we observed that B cells naive, T cells CD8, T cells follicular helper, T cells regulatory Tregs, NK cells activated, Monocytes, Macrophages M1, and Mast cells activated were more abundant in the low-risk subgroup, while plasma cells and Macrophages M2 were more abundant in the high-risk subgroup (Fig. 5F). TME scores including the stromal score and immune score were significantly higher in the high-risk subgroup (Fig. 5G). ICGs including *CD274*, *CD27*, *CD28*, *CD40*, *CD48*, *ICOS*, *TIGIT*, *LGALS9*, *PVR* and *CD226* were significantly expressed higher in the high-risk subgroup (Fig. 5H).

3.7. Estimation of immunotherapy response and chemotherapeutic sensitivity in different risk score subgroups

The TIDE algorithm was utilized to evaluate the potential clinical effectiveness of immunotherapy across different risk score subgroups. Higher integrated TIDE score indicated an increased likelihood of immune evasion, implying that patients with elevated scores are less likely to derive benefits from immunotherapy. Our findings revealed that the TIDE score in the low-risk group was significantly lower compared to that in the high-risk group, suggesting that low-risk patients may gain more advantages from immunotherapy than high-risk patients (Fig. 6A). We also found that the low-risk subgroup had a higher MSI score, while the high-risk subgroup had higher T cell dysfunction and exclusion score. Patients categorized with a combination of a low-risk score and a high TIDE score exhibited the most favorable prognosis. In contrast, those with a high-risk score coupled with a low TIDE score demonstrated the worst prognosis (Fig. 6B). Then, we conducted a validation of the predictive efficacy of the cuproptosis-related risk prognostic model within the IMvigor210 cohort. CCA patients were divided into low- and high-risk groups based on the previously constructed risk prognostic model. The Kaplan-Meier curve revealed that patients with low-risk score had a better OS than those with high-risk score (Fig. 6C). Furthermore, CCA patients in the low-risk group were more likely to benefit from immunotherapy (Fig. 6D and E). The distribution of patients by risk score, immunotherapy response, and survival status in the IMvigor210 cohort (Fig. 6F). We then further investigated the risk score values to assess their potential as biomarkers for predicting the chemotherapeutic responses in patients with CCA. Higher imputed sensitivity score indicated a lower sensitivity to the drug. In our results, we found patients in the low-risk group had a lower IC50 in oxaliplatin, palbociclib, sabutoclax, uprosertib, and afuresertib, while the IC50 in savolitinib, trametinib, and ulixertinib were lower in the high-risk group (Fig. 6G).

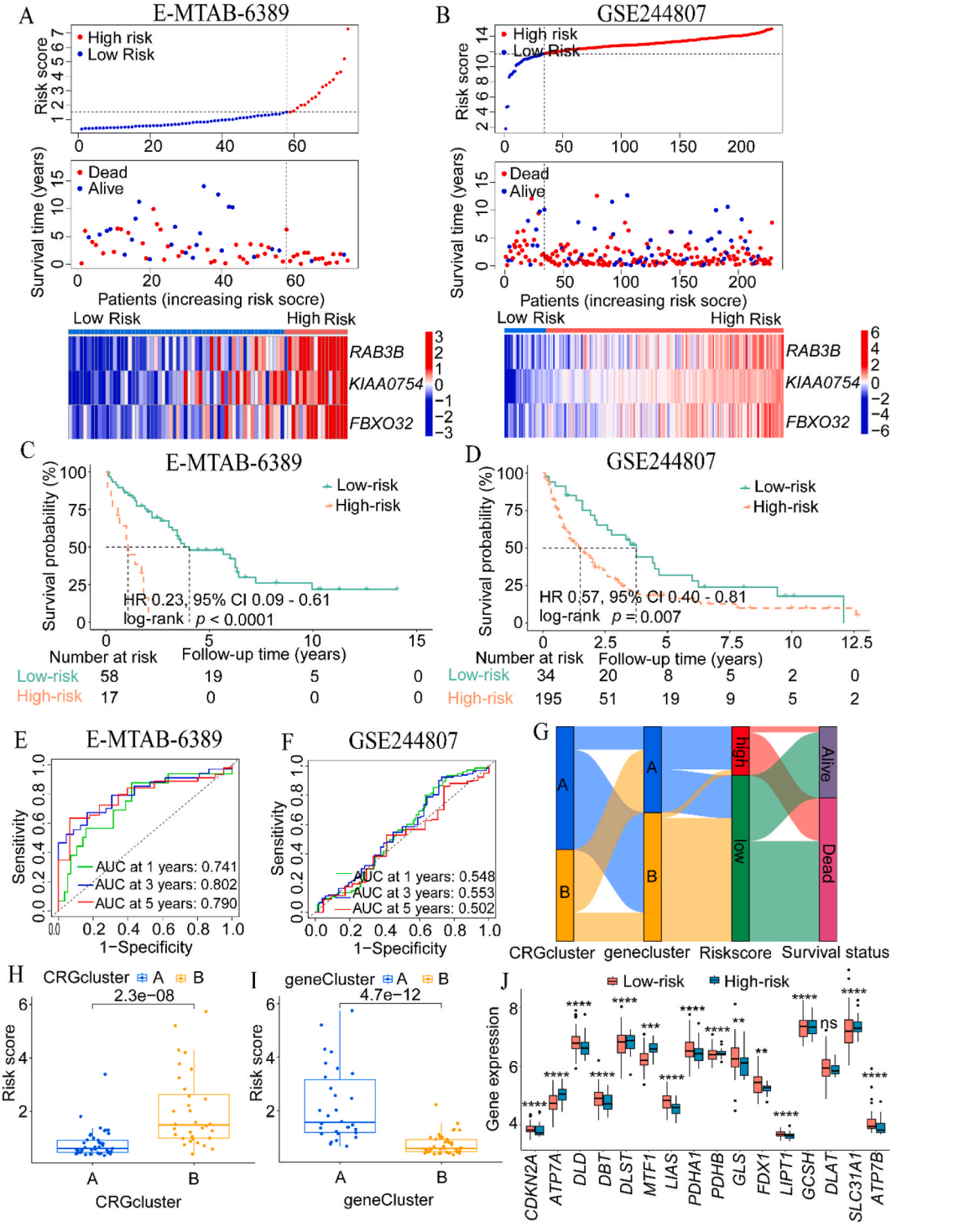

(caption on next page)

Fig. 4. Evaluation of the cuproptosis-related risk prognostic model in the E-MTAB-6389 cohort and validation in GSE244807 cohort in CCA. (A) The distribution of risk score, survival status, and the expression of three genes in the cuproptosis-related risk prognostic model in E-MTAB-6389 cohort. (B) The distribution of risk score, survival status, and the expression of three genes in the cuproptosis-related risk prognostic model in GSE244807 cohort. (C) The Kaplan-Meier OS curves for patients in the high- and low-risk groups in the E-MTAB-6389 cohort. (D) The Kaplan-Meier OS curves for patients in the high- and low-risk groups in the GSE244807 cohort. (E) ROC curves showed the prognostic performance of the cuproptosis-related risk prognostic model in the E-MTAB-6389 cohort. (F) ROC curves showed the prognostic performance of the cuproptosis-related risk prognostic model in the GSE244807 cohort. (G) Sankey diagram of subtype distributions in groups with different risk scores and survival outcomes. (H) Differences in risk scores between CRG clusters. (I) Differences in risk scores between gene clusters. (J) Differential expression of CRGs between high- and low-risk groups. CRGs: cuproptosis-related genes; ROC, receiver operating characteristic; OS, overall survival; ns: not significant, $^{**}p < 0.01$, $^{***}p < 0.001$, $^{****}p < 0.0001$.

3.8. Quantitative real-time PCR, and western blotting

The expression levels of the three key genes in CCA were further validate by qRT-PCR and WB on normal intrahepatic bile duct cell (HIBEC) and CCA cells (HUCCT1 and RBE). As shown in Fig. 7A–C, qRT-PCR showed that the expression of the *RAB3B*, *KIAA0754*, and *FBXO32* were significantly upregulated in tumor cells. The results of WB also demonstrated a consistent significant upregulated in *RAB3B*, *KIAA0754*, and *FBXO32* at the protein level (Fig. 7D).

4. Discussion

Cuproptosis is a unique form of cell death that is dependent on copper and distinct from other known types of cell death, and was first proposed by Tsvetkov et al. [13]. The mechanism underlying cuproptosis was believed to involve interactions with components of the TCA cycle within mitochondria, leading to the accumulation of copper ions in cells. This accumulation induces a conserved post-transcriptional protein modification pathway and lipoylation [13]. Furthermore, studies have indicated a significant increase in serum copper ion levels in tumor tissues compared to normal, like lung cancer [9], breast cancer [10], carcinoma of gallbladder [11]. Recently, plenty of studies have focused on the crucial role of the cuproptosis in both tumor development and patient prognosis. However, due to the high malignancy, rapid progression, and lack of effective treatments in CCA patients, there is an urgent need to develop effective diagnostic and prognostic biomarkers for precise therapy. Therefore, the association between CRGs and prognosis in CCA still remain to be further illustrated.

In the present study, we systematically investigated the molecular characteristic of 16 CRGs at genetic and transcriptional variations in CCA. We found that *CDKN2A* had the highest mutation frequency, followed by *MTF1*, *LIAS* and *ATP7B*, as reported previously [24]. We observed that the CNV levels exhibited significant differences in relation to the expression of CRGs, suggesting a potential contribution of CNV to the heterogeneity of CRGs in CCA. Then, we investigated the differentially expressed CRGs between normal and tumor samples, uncovering that 11 CRGs were significantly upregulated in tumor samples when compared to normal. Furthermore, the results from GO and KEGG analyses indicated that these CRGs were particularly enriched in TCA cycle, pyruvate metabolism, glycolysis, as well as copper ion import; this aligns with findings from numerous studies that have highlighted the significance of copper metabolism in cancer [25]. Moreover, we found that the expression of the majority of CRGs were significantly correlated with patient prognosis. Highly expressed *ATP7B*, *CDKN2A*, *FDX1*, and *LIAS* were steadily associated with better prognosis in CCA patients, while *ATP7A*, *PDHA1*, and *SLC31A1* were the opposite. Subsequently, we identified six significant prognostic genes by multivariate cox regression. *FDX1*, a key gene that promotes copper induced death, and its deletion play a crucial role in inducing protein lipoylation, which subsequently leads to resistance against cuproptosis [26]. *PDHA1* was an anti-cuproptosis genes, which plays a role in hepatocellular carcinoma cancer metastasis and clinical pathology [27].

Based on the expression profile of CRGs, we further classified CCA patients into two distinct molecular subtypes. Moreover, a majority of the CRGs exhibit differential expression between different CRG clusters. Additionally, the patients in cluster A subgroup had a better prognosis and less death events than patients in cluster B. These findings suggest that the observed differences could be partially ascribed to different responses to treatment in CCA. To substantiate this hypothesis, we further analyzed the patterns of immune cell infiltration and the expression of immune checkpoint genes between two clusters. Compared to patients with cluster A, patients with subtype B significantly enriched in notch signaling pathway, cell cycle, Fc gamma r mediated phagocytosis and pancreatic cancer, which were found to be involved in the cell proliferation and progression of CCA [28]. In addition, cluster B-related genes were mainly enriched in geneCluster A, which may be associated with pathways related to promoting tumor progression; moreover, patients in geneCluster B subgroup had a better prognosis than patients in geneCluster A, consistent with the above results. We also found striking differences in dendritic cell, natural killer cell, type 17 T helper cell and type 2 T helper cell, StromalScore and ImmuneScore between clusters. Previous studies have shown that the CCA microenvironment is 'immune cold', with a paucity of cytotoxic immune cells and an abundance of immunosuppressive elements, especially myeloid cells [29]. Higher TIDE score indicated that patients were less likely to benefit from immunotherapy [22]. In contrast, patients classified in cluster A exhibit a lower integrated TIDE score, suggesting they may be sensitive to ICIs. These findings demonstrate a significant relationship between cuproptosis and tumor immunity, highlighting the potential implications of cuproptosis in the prognosis and treatment of CCA.

Previous studies have demonstrated a correlation between programmed cell death-related phenotypes and CCA, and corresponding prognostic models have been established [30,31]. However, whether cuproptosis was also an important indicator for prognostic prediction in CCA at the transcriptomic level needs to be further investigated. Two distinct genomic subtypes were identified based on the OS-associated DEGs. Furthermore, genomic subtypes demonstrated a strong correlation with patient prognosis, highlighting its

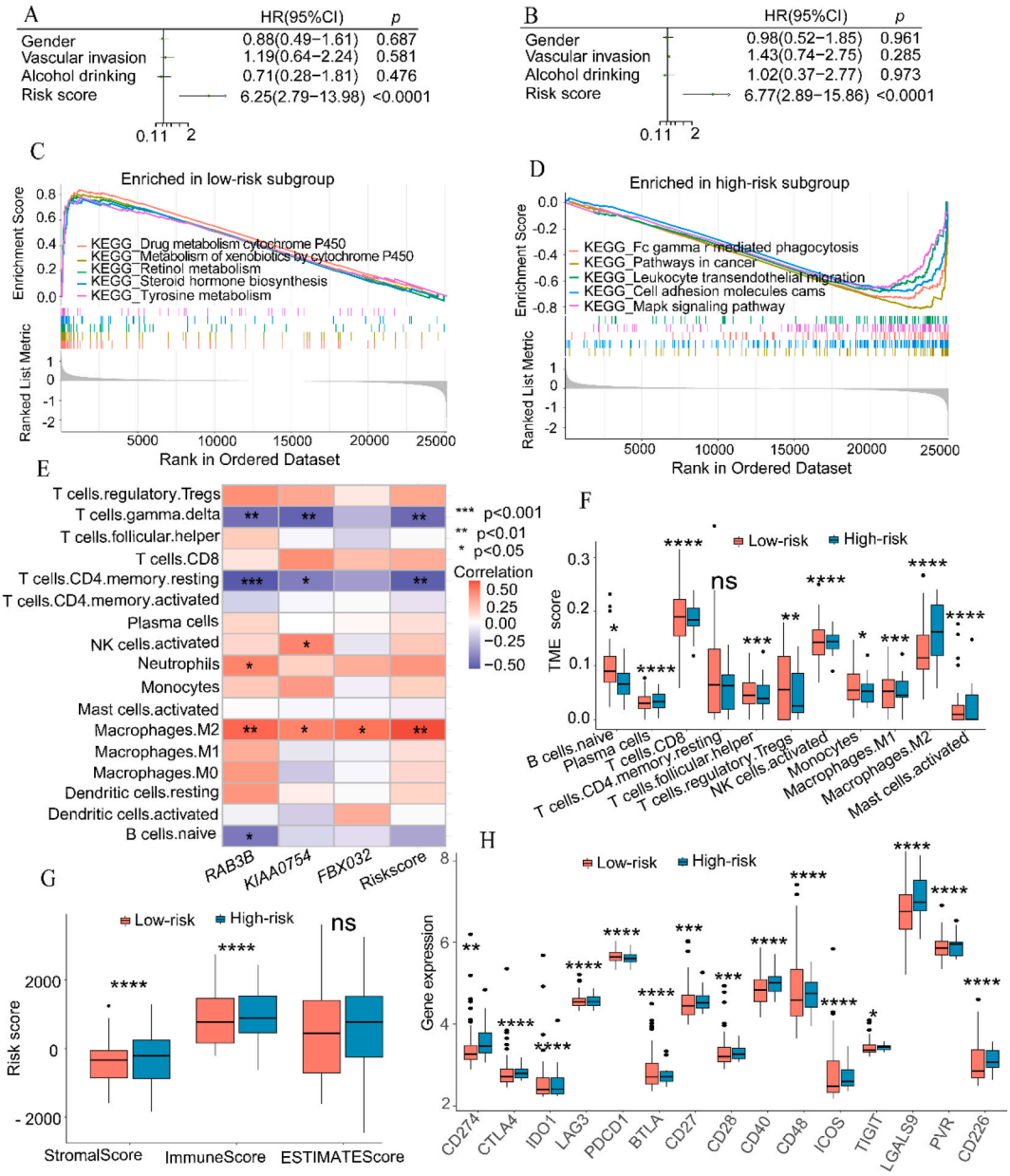

Fig. 5. Evaluation of the risk score prognostic model with clinical application, tumor microenvironment, and immune checkpoint genes (ICGs) in the E-MTAB-6389 cohort. The forest plot for univariate Cox (A) and multivariate Cox regression (B) considering clinical indicators and risk score in CCA. Gene set enrichment analysis (GSEA) enriched in low-risk group (C) and high-risk group (D). (E) Correlations between the abundance of immune cells and three genes and risk score. (F) Difference in the abundance of immune cells between high- and low-risk groups. (G) Immune-stromal component evaluation of the high- and low-risk groups. (H) The different expressions of ICGs between high- and low-risk groups. ns: not significant, $*p < 0.05$, $**p < 0.01$, $***p < 0.001$, $****p < 0.0001$.

predictive capacity for CCA. In order to better evaluate the cuproptosis pattern in individual CCA patients, we have developed a novel prognostic model that was based on 3 cuproptosis-related genes (namely, *RAB3B*, *KIAA0754*, *FBXO32*). *RAB3B*, one of the low-molecular-weight GTP-binding proteins (small G proteins) in the *Rab* family, and acts as a central regulator of vesicular traffic [32]. A study showed that the up regulation of *RAB3B* may play an important role in the sphere formation, chemoresistance, and metastatic potential of hepatoma cells [33]. *KIAA0754*, also known as *MACF1* (microtubule actin cross-linking factor 1), was a multidomain protein that can associate with microfilaments and microtubules. Zhang et al. showed that m6A modification level and expression of potential driver gene *MACF1* could be regulated by *METTL14*, which can influence the proliferation and metastasis ability of CCA cells [34]. *FBXO32*, a component of the *SCF E3* ligase complex, was shown to favor breast cancer cell xenograft development, and its overexpression was associated with poor prognosis [35]. Another study showed that *FBXO32* favors melanoma

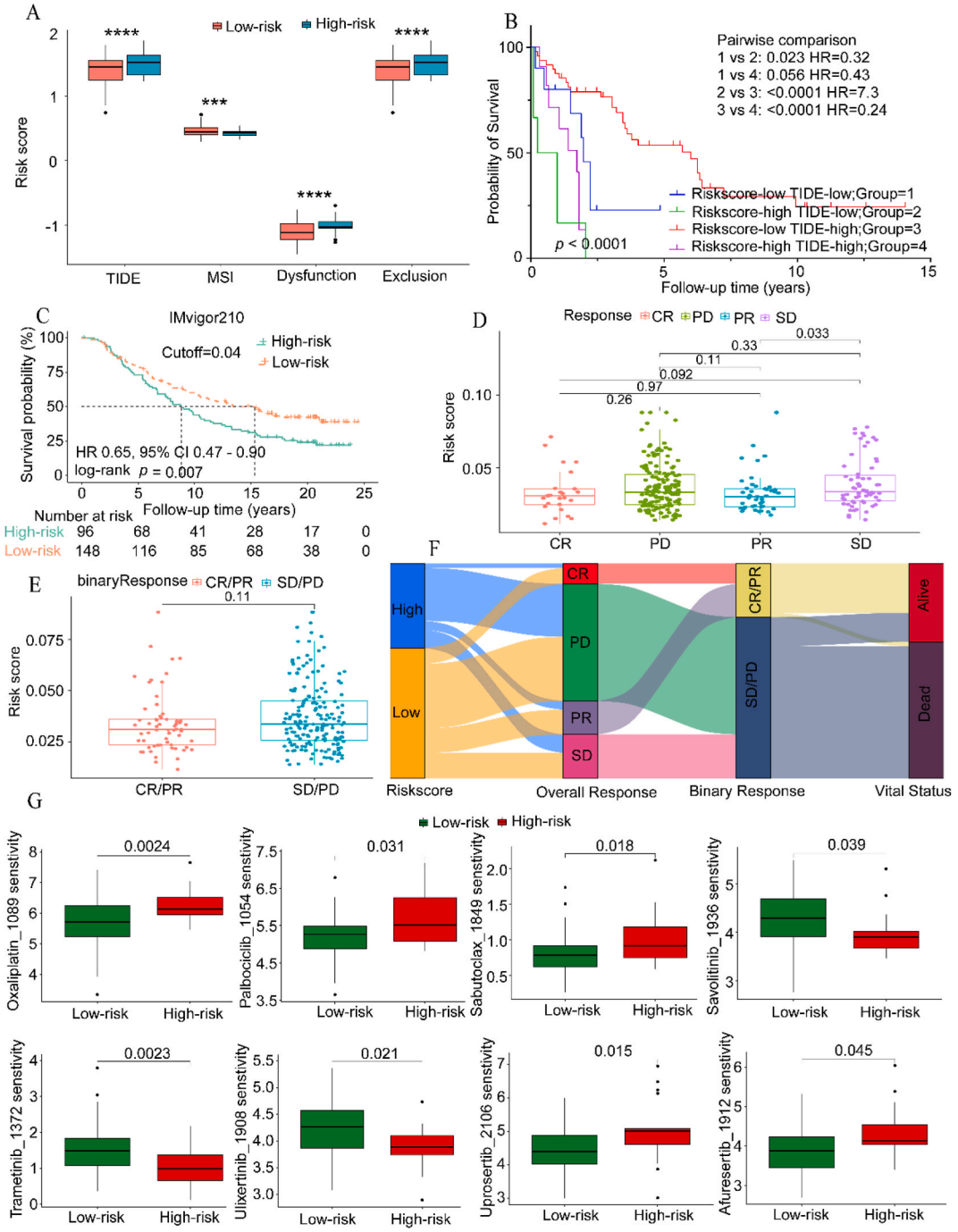

Fig. 6. Estimation of the risk score prognostic model in immunotherapy response and chemotherapeutic sensitivity in CCA. (A) Tumor immune dysfunction and exclusion (TIDE) score between high- and low-risk groups. (B) The Kaplan-Meier OS curves among four groups classified by the risk score and TIDE score. (C) The Kaplan-Meier OS curves for patients in the high- and low-risk groups in the IMvigor210 cohort. (D) Difference in risk scores among four immunotherapy response groups in the IMvigor210 cohort. (E) Difference in risk scores between binary response groups. (F) Sankey diagram of subtype distributions in groups with different risk scores and immunotherapy response in the IMvigor210 cohort. (G) Difference in chemotherapeutic sensitivity between high- and low-risk groups in the E-MTAB-6389 cohort. ***$p < 0.001$, ****$p < 0.0001$; CR: complete response; PR: partial response; PD: progressive disease; SD: stable disease; OS, overall survival.

cell migration, proliferation, and tumor development in vivo [36].

In our study, the distribution plots and K-M plot showed that the patients in the high-risk subgroup had a shorter OS than patients in the low-risk group in the E-MTAB training and validation cohorts. Furthermore, the risk score was tested as an independent signature

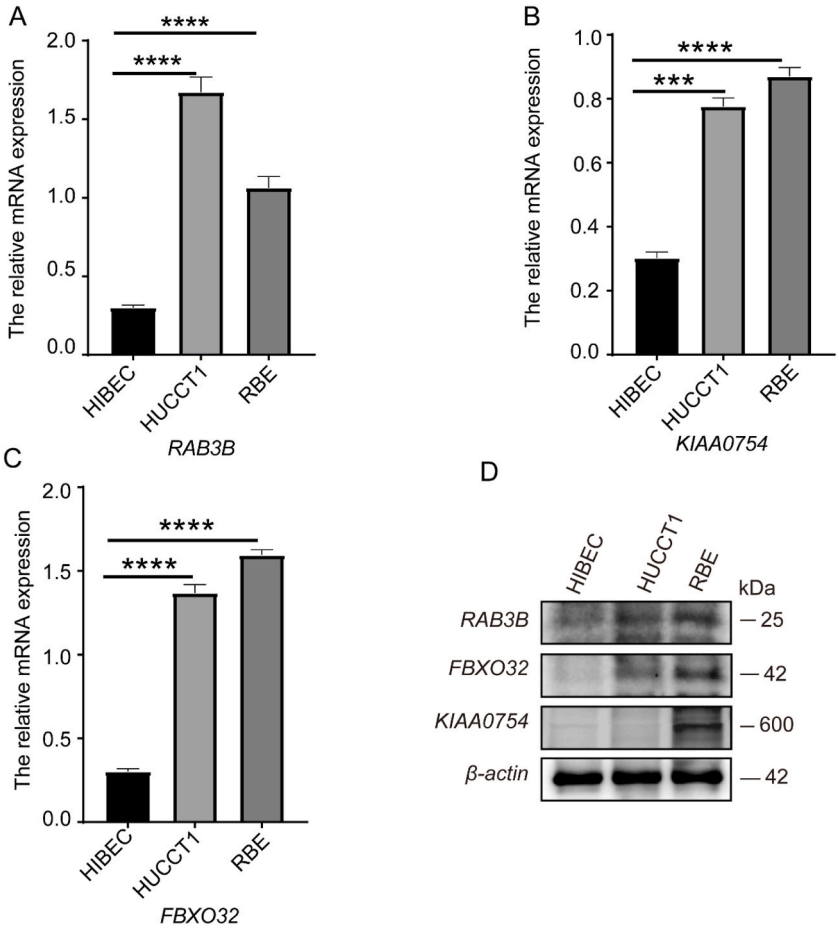

Fig. 7. The expressions of three signature genes were validated by quantitative real-time PCR (qRT-PCR) and Western blotting (WB). (A–C) RT-qPCR was performed to detect the expression of *RAB3B*, *KIAA0754*, and *FBXO32* in normal intrahepatic bile duct cell (HIBEC) and CCA cells (HUCCT1 and RBE). (D) Expression of genes at the protein level by WB. ***$p < 0.001$, ****$P < 0.0001$.

for CCA patients, and the AUC value of the signature in predicting prognosis showed satisfactory predictive ability. Meanwhile, patients with CRG cluster B and gene cluster A exhibited a higher risk score and the worst outcomes, and a higher risk score was usually accompanied by higher expression levels of CRGs with poor outcomes in CCA tissues. We further validated the expression of these 3 genes in qRT-PCR and WB ways. The qRT-PCR and WB results showed that *RAB3B*, *KIAA0754*, and *FBXO32* were significantly upregulated in CCA cells than in normal cell in both the mRNA and protein levels. Taken together, these results indicated that the scoring system's has independent and robust prognostic-predictive ability in CCA.

Cancer immunotherapy has garnered significant attention due to the crucial role of immunobiology in the development of malignant processes. Additionally, cuproptosis is closely linked to the regulation of anti-tumor immunity, a comprehensive understanding of cuproptosis in the TME and its impact on cell infiltration could enhance the effectiveness of CCA antitumor therapies and guiding more effective immunotherapy strategies [37]. In this study, GSEA enrichment analysis illustrated that high-risk subgroup was involved in cancer, cell adhesion and migration. Risk score signature was found to be significantly positively correlated with M2 macrophages. The composition of some immune cells was different between two risk score subgroups. B cells naive, T cells CD8, T cells follicular helper, NK cells activated, Macrophages M1, and Mast cells activated were more abundant in the low-risk subgroup, while Macrophages M2 were more abundant in the high-risk subgroup. In addition, higher stromal score, higher immunescore, and most ICGs exhibited a higher risk score. Previous studies have revealed that M2 macrophages, a predominant subtype of macrophages, have been proven to be correlate with chronic inflammation and promote tumor growth and invasiveness, these cells have been associated with a poor outcome in intrahepatic cholangiocarcinoma [38,39]. Loeuillard et al. showed that tumor-associated macrophages as the primary source of programmed death-ligand 1 (PD-L1) in human and murine CCA and facilitated CCA progression [40]. Liu et al. showed that $CD8^+$ and $CD4^+$ T cells, and $CD20^+$ B cells are positively correlated with the prognosis of CCA [41]. The findings of our study corroborate these conclusions. Furthermore, the high-risk samples exhibited a greater presence of immunosuppressive cells as well as signals associated with tumor development and metastasis, which suggested that high-risk subgroup was characterized by immunosuppression and active tumor progression. Therefore, high-risk subgroup has a worse outcome than low-risk subgroup, in agreement with above survival results.

The TIDE prediction score exhibited a correlation with T cell dysfunction in tumors characterized by cytotoxic lymphocytes (CTL)-high and T cell exclusion in tumors with CTL-low, thus representing the existence of two distinct immune escape mechanisms [22]. In our study, compared to low-risk patients, high-risk patients had less CTL infiltration, higher TIDE, T cell exclusion and T cell dysfunction score, so their diminished ICI response might be attributed to immune evasion via T cell exclusion and dysfunction [22]. In contrast, the low-risk subgroup had a lower TIDE score along with a higher MSI score compared to the high-risk subgroup, which suggested that patients in the low-risk subgroup may be more likely to benefit from ICI. To further validate the prognostic significance of the risk score, we conducted survival analysis in the IMvigor210 cohort, which is comprised of patients undergoing immunotherapy. We discovered that the risk score effectively distinguishes different outcomes in patients undergoing immunotherapy, with those classified as low-risk demonstrating a greater likelihood of benefiting from the treatment.

A review showed that targeting copper-related cell metabolism was a promising strategy for cancer treatment [42]. In this study, we aimed to predict the responses of 8 drugs in CCA. Higher imputed sensitivity score indicated a lower sensitivity to the corresponding drug. We found that low-risk subtype patients were more sensitive to oxaliplatin, palbociclib, sabutoclax, uprosertib, and afuresertib than high-risk subtype patients. A previous clinical study showed that the combination of gemcitabine with oxaliplatin has favorable clinical efficacy and toxicity profile [43]. A case report showed that a 68-year-old patient with metastasis ICC harboring CDKN2A/B loss, who achieved a partial response (PR) after the first-line treatment with a CDK4/6 inhibitor called palbociclib [44]. Results showed that targeting CRGs might contribute to enhancing therapeutic effects of CCA patients.

Nevertheless, our study also showed some limitations. First, the CRG risk signature was performed based on data obtained retrospectively from public databases, which was inevitably limited by inherent case selection bias. More large-scale prospective clinical studies and samples of clinic tissues are needed to confirm our findings. Second, some datasets are missing some critical clinical variables, such as chemotherapy and immunotherapy, which may affect the results of treatment response and cuproptosis state analyses. Finally, more clinicopathologic samples should be included to validate the correlation between the expression of key CRGs and immune markers (such as CD8 and PD-L1), and more in vivo or *in vitro* functional experiments are needed in the future to validate the roles of the signature genes.

5. Conclusion

In conclusion, we have detailed the molecular characterization of CRGs in CCA and developed a novel risk model that aids in predicting the prognosis and treatment for CCA patients, which was partially constituted by a 3-CRG signature (*RAB3B*, *KIAA0754* and *FBXO32*).

CRediT authorship contribution statement

Liye Wang: Writing – review & editing, Writing – original draft, Software, Methodology, Funding acquisition, Data curation, Conceptualization. **Pan Li:** Writing – review & editing, Writing – original draft, Software, Methodology, Investigation, Data curation. **Shuai Gong:** Writing – review & editing, Methodology, Formal analysis, Data curation. **Lina Pang:** Writing – review & editing, Software, Methodology, Formal analysis. **Mingyu Li:** Writing – review & editing, Software, Methodology, Data curation. **Chi Zhang:** Writing – review & editing, Methodology, Investigation, Data curation. **Shengli Zhang:** Writing – review & editing, Resources, Project administration, Formal analysis. **Xiaoke Zhang:** Writing – review & editing, Supervision, Methodology, Data curation. **Guozhong Jiang:** Writing – review & editing, Software, Methodology, Data curation. **Wei He:** Writing – review & editing, Writing – original draft, Supervision, Software, Methodology, Data curation, Conceptualization.

Ethics approval and consent to participate

Not applicable.

Consent for publication

All authors consent to the publication of this study.

Availability of data and materials

Publicly available datasets were analyzed in this study. This data can be found here: TCGA: https://portal.gdc.cancer.gov/; E-MTAB-6389: https://www.ebi.ac.uk/arrayexpress/; GSE244807:https://www.ncbi.nlm.nih.gov/geo/query/acc.cgi?acc=GSE244807; IMvigor210: http://research-pub.gene.com/IMvigor210CoreBiologies.

Funding

This work was supported by Natural Science Foundation of Henan (242300421482) and He'nan Educational Committee (25A320069).

Declaration of competing interest

None of the authors have financial or other contractual agreements that might cause conflicts of interest.

Appendix A. Supplementary data

Supplementary data to this article can be found online at https://doi.org/10.1016/j.heliyon.2024.e41600.

References

[1] P.M. Rodrigues, P. Olaizola, N.A. Paiva, et al., Pathogenesis of cholangiocarcinoma, Annu. Rev. Pathol. 16 (Jan 24 2021) 433–463, https://doi.org/10.1146/annurev-pathol-030220-020455.

[2] J.M. Banales, J.J.G. Marin, A. Lamarca, et al., Cholangiocarcinoma 2020: the next horizon in mechanisms and management, Nat. Rev. Gastroenterol. Hepatol. 17 (9) (Sep 2020) 557–588, https://doi.org/10.1038/s41575-020-0310-z.

[3] A. Lamarca, D.H. Palmer, H.S. Wasan, et al., Second-line FOLFOX chemotherapy versus active symptom control for advanced biliary tract cancer (ABC-06): a phase 3, open-label, randomised, controlled trial, Lancet Oncol. 22 (5) (May 2021) 690–701, https://doi.org/10.1016/S1470-2045(21)00027-9.

[4] P.J. Brindley, M. Bachini, S.I. Ilyas, et al., Cholangiocarcinoma, Nat. Rev. Dis. Prim. 7 (1) (Sep 9 2021) 65, https://doi.org/10.1038/s41572-021-00300-2.

[5] S.I. Ilyas, S. Affo, L. Goyal, et al., Cholangiocarcinoma - novel biological insights and therapeutic strategies, Nat. Rev. Clin. Oncol. 20 (7) (Jul 2023) 470–486, https://doi.org/10.1038/s41571-023-00770-1.

[6] R.A. Festa, D.J. Thiele, Copper: an essential metal in biology, Curr. Biol. 21 (21) (Nov 8 2011) R877–R883, https://doi.org/10.1016/j.cub.2011.09.040.

[7] P.A. Cobine, S.A. Moore, S.C. Leary, Getting out what you put in: copper in mitochondria and its impacts on human disease, Biochim. Biophys. Acta Mol. Cell Res. 1868 (1) (Jan 2021) 118867, https://doi.org/10.1016/j.bbamcr.2020.118867.

[8] J. Xie, Y. Yang, Y. Gao, J. He, Cuproptosis: mechanisms and links with cancers, Mol. Cancer 22 (1) (Mar 7 2023) 46, https://doi.org/10.1186/s12943-023-01732-y.

[9] W. Wang, X. Wang, J. Luo, et al., Serum copper level and the copper-to-zinc ratio could Be useful in the prediction of lung cancer and its prognosis: a case-control study in northeast China, Nutr. Cancer 73 (10) (2021) 1908–1915, https://doi.org/10.1080/01635581.2020.1817957.

[10] V. Pavithra, T.G. Sathisha, K. Kasturi, D.S. Mallika, S.J. Amos, S. Ragunatha, Serum levels of metal ions in female patients with breast cancer, J. Clin. Diagn. Res. 9 (1) (Jan 2015) BC25–c27, https://doi.org/10.7860/JCDR/2015/11627.5476.

[11] S. Basu, M.K. Singh, T.B. Singh, S.K. Bhartiya, S.P. Singh, V.K. Shukla, Heavy and trace metals in carcinoma of the gallbladder, World J. Surg. 37 (11) (Nov 2013) 2641–2646, https://doi.org/10.1007/s00268-013-2164-9.

[12] H. Liu, L. Xu, Y. Zhang, et al., Copper increases the sensitivity of cholangiocarcinoma cells to tripterine by inhibiting TMX2-mediated unfolded protein reaction activation, Adv Healthc Mater 12 (26) (Oct 2023) e2300913, https://doi.org/10.1002/adhm.202300913.

[13] P. Tsvetkov, S. Coy, B. Petrova, et al., Copper induces cell death by targeting lipoylated TCA cycle proteins, Science (New York, NY) 375 (6586) (Mar 18 2022) 1254–1261, https://doi.org/10.1126/science.abf0529.

[14] D. Tang, X. Chen, G. Kroemer, Cuproptosis: a copper-triggered modality of mitochondrial cell death, Cell Res. 32 (5) (May 2022) 417–418, https://doi.org/10.1038/s41422-022-00653-7.

[15] J.H. Bao, W.C. Lu, H. Duan, et al., Identification of a novel cuproptosis-related gene signature and integrative analyses in patients with lower-grade gliomas, Front. Immunol. 13 (2022) 933973, https://doi.org/10.3389/fimmu.2022.933973.

[16] X. Qi, J. Guo, G. Chen, et al., Cuproptosis-related signature predicts the prognosis, tumor microenvironment, and drug sensitivity of hepatocellular carcinoma, Journal of immunology research 2022 (2022) 3393027, https://doi.org/10.1155/2022/3393027.

[17] A.M. Bolger, M. Lohse, B. Usadel, Trimmomatic: a flexible trimmer for Illumina sequence data, Bioinformatics 30 (15) (Aug 1 2014) 2114–2120, https://doi.org/10.1093/bioinformatics/btu170.

[18] H. Li, B. Handsaker, A. Wysoker, et al., The sequence alignment/map format and SAMtools, Bioinformatics 25 (16) (Aug 15 2009) 2078–2079, https://doi.org/10.1093/bioinformatics/btp352.

[19] F. Ramirez, D.P. Ryan, B. Gruning, et al., deepTools2: a next generation web server for deep-sequencing data analysis, Nucleic Acids Res. 44 (W1) (Jul 8 2016) W160–W165, https://doi.org/10.1093/nar/gkw257.

[20] R.L. Camp, M. Dolled-Filhart, D.L. Rimm, X-tile: a new bio-informatics tool for biomarker assessment and outcome-based cut-point optimization, Clin. Cancer Res. 10 (21) (Nov 1 2004) 7252–7259, https://doi.org/10.1158/1078-0432.CCR-04-0713.

[21] J.P. Brunet, P. Tamayo, T.R. Golub, J.P. Mesirov, Metagenes and molecular pattern discovery using matrix factorization, Proc Natl Acad Sci U S A. 101 (12) (Mar 23 2004) 4164–4169, https://doi.org/10.1073/pnas.0308531101.

[22] P. Jiang, S. Gu, D. Pan, et al., Signatures of T cell dysfunction and exclusion predict cancer immunotherapy response, Nature medicine 24 (10) (Oct 2018) 1550–1558, https://doi.org/10.1038/s41591-018-0136-1.

[23] S. Mariathasan, S.J. Turley, D. Nickles, et al., TGFbeta attenuates tumour response to PD-L1 blockade by contributing to exclusion of T cells, Nature 554 (7693) (Feb 22 2018) 544–548, https://doi.org/10.1038/nature25501.

[24] C. Zhang, X. You, Q. Zhang, D. Wang, Molecular profiling and prognostic analysis in Chinese cholangiocarcinoma: an observational, retrospective single-center study, Invest. N. Drugs (Nov 17 2023), https://doi.org/10.1007/s10637-023-01394-z.

[25] Y. Qin, Y. Liu, X. Xiang, et al., Cuproptosis correlates with immunosuppressive tumor microenvironment based on pan-cancer multiomics and single-cell sequencing analysis, Mol. Cancer 22 (1) (Mar 24 2023) 59, https://doi.org/10.1186/s12943-023-01752-8.

[26] Y. Wang, L. Zhang, F. Zhou, Cuproptosis: a new form of programmed cell death, Cell. Mol. Immunol. 19 (8) (Aug 2022) 867–868, https://doi.org/10.1038/s41423-022-00866-1.

[27] J. Sun, J. Li, Z. Guo, et al., Overexpression of pyruvate dehydrogenase E1alpha subunit inhibits warburg effect and induces cell apoptosis through mitochondria-mediated pathway in hepatocellular carcinoma, Oncology research 27 (4) (Mar 29 2019) 407–414, https://doi.org/10.3727/096504018X15180451872087.

[28] G. Zhou, H. He, X. Wang, Q. Gu, LncRNA-HANR exacerbates malignant behaviors of cholangiocarcinoma cells through activating Notch pathway, Heliyon 9 (12) (Dec 2023) e22087, https://doi.org/10.1016/j.heliyon.2023.e22087.

[29] G. Zhou, D. Sprengers, S. Mancham, et al., Reduction of immunosuppressive tumor microenvironment in cholangiocarcinoma by ex vivo targeting immune checkpoint molecules, Journal of hepatology 71 (4) (Oct 2019) 753–762, https://doi.org/10.1016/j.jhep.2019.05.026.

[30] L. Xu, X. Gao, J. Xing, Z. Guo, Identification of a necroptosis-related gene signature as a novel prognostic biomarker of cholangiocarcinoma, Front. Immunol. 14 (2023) 1118816, https://doi.org/10.3389/fimmu.2023.1118816.

[31] Z.J. Zhang, Y.P. Huang, X.X. Li, et al., A novel ferroptosis-related 4-gene prognostic signature for cholangiocarcinoma and photodynamic therapy, Front. Oncol. 11 (2021) 747445, https://doi.org/10.3389/fonc.2021.747445.

[32] P.M. Lledo, P. Vernier, J.D. Vincent, W.T. Mason, R. Zorec, Inhibition of Rab3B expression attenuates Ca(2+)-dependent exocytosis in rat anterior pituitary cells, Nature 364 (6437) (Aug 5 1993) 540–544, https://doi.org/10.1038/364540a0.

[33] R. Tsunedomi, K. Yoshimura, Y. Kimura, et al., Elevated expression of RAB3B plays important roles in chemoresistance and metastatic potential of hepatoma cells, BMC Cancer 22 (1) (Mar 11 2022) 260, https://doi.org/10.1186/s12885-022-09370-1.
[34] Y. Zhang, Z. Ma, C. Li, et al., The genomic landscape of cholangiocarcinoma reveals the disruption of post-transcriptional modifiers, Nat. Commun. 13 (1) (Jun 1 2022) 3061, https://doi.org/10.1038/s41467-022-30708-7.
[35] S.K. Sahu, N. Tiwari, A. Pataskar, et al., FBXO32 promotes microenvironment underlying epithelial-mesenchymal transition via CtBP1 during tumour metastasis and brain development, Nat. Commun. 8 (1) (Nov 15 2017) 1523, https://doi.org/10.1038/s41467-017-01366-x.
[36] N. Habel, N. El-Hachem, F. Soysouvanh, et al., FBXO32 links ubiquitination to epigenetic reprograming of melanoma cells, Cell Death Differ. 28 (6) (Jun 2021) 1837–1848, https://doi.org/10.1038/s41418-020-00710-x.
[37] W.Q. Liu, W.R. Lin, L. Yan, W.H. Xu, J. Yang, Copper homeostasis and cuproptosis in cancer immunity and therapy, Immunol. Rev. (Sep 16 2023), https://doi.org/10.1111/imr.13276.
[38] H. Yuan, Z. Lin, Y. Liu, et al., Intrahepatic cholangiocarcinoma induced M2-polarized tumor-associated macrophages facilitate tumor growth and invasiveness, Cancer Cell Int. 20 (1) (Dec 7 2020) 586, https://doi.org/10.1186/s12935-020-01687-w.
[39] D. Sun, T. Luo, P. Dong, et al., M2-polarized tumor-associated macrophages promote epithelial-mesenchymal transition via activation of the AKT3/PRAS40 signaling pathway in intrahepatic cholangiocarcinoma, J. Cell. Biochem. 121 (4) (Apr 2020) 2828–2838, https://doi.org/10.1002/jcb.29514.
[40] E. Loeuillard, J. Yang, E. Buckarma, et al., Targeting tumor-associated macrophages and granulocytic myeloid-derived suppressor cells augments PD-1 blockade in cholangiocarcinoma, The Journal of clinical investigation 130 (10) (Oct 1 2020) 5380–5396, https://doi.org/10.1172/JCI137110.
[41] D. Liu, L.R. Heij, Z. Czigany, et al., The role of tumor-infiltrating lymphocytes in cholangiocarcinoma, Journal of experimental & clinical cancer research : CR 41 (1) (Apr 7 2022) 127, https://doi.org/10.1186/s13046-022-02340-2.
[42] R. Kong, G. Sun, Targeting copper metabolism: a promising strategy for cancer treatment, Front. Pharmacol. 14 (2023) 1203447, https://doi.org/10.3389/fphar.2023.1203447.
[43] T. Andre, C. Tournigand, O. Rosmorduc, et al., Gemcitabine combined with oxaliplatin (GEMOX) in advanced biliary tract adenocarcinoma: a GERCOR study, Ann. Oncol. 15 (9) (Sep 2004) 1339–1343, https://doi.org/10.1093/annonc/mdh351.
[44] W. Fan, C. Wang, X. Zhong, et al., A refractory case of CDKN2A/B loss metastatic intrahepatic cholangiocarcinoma achieving a partial response after first-line treatment with palbociclib, OncoTargets Ther. 16 (2023) 23–29, https://doi.org/10.2147/OTT.S390458.